DISSIPATIVE PARTICLE DYNAMICS SIMULATION OF MULTIPLE DEFORMABLE RED BLOOD CELLS IN A VESSEL

LANLAN XIAO[1, 2], YANG LIU[2], SHUO CHEN[1, *] & BINGMEI FU[3]
[1]School of Aerospace Engineering and Applied Mechanics, Tongji University, Shanghai, China.
[2]Department of Mechanical Engineering, The Hong Kong Polytechnic University, Hong Kong, China.
[3]Department of Biomedical Engineering, The City College of the City University of New York, New York, NY, USA.
*Email: schen_tju@tongji.edu.cn

ABSTRACT
The blood flow properties in microvessels were examined through simulating the dynamics of deformable red blood cells suspended in plasma using dissipative particle dynamics. The cell membrane was considered as a spring-based triangulated network and the intercellular interaction was modeled by a Morse potential function. The cell distribution in the cross section indicated that red blood cells migrate away from the wall to the tube center, resulting in a cell-free layer near the wall and blunt velocity profile. The findings also showed that the bluntness of velocity profile increases with increasing hematocrit. In addition, the Fahraeus and Fahraeus–Lindqvist effects were captured through investigating the effects of tube diameter and hematocrit on the discharge hematocrit and relative apparent viscosity. It appears that this flow model can capture the blood flow behaviors under physiological and pathological conditions.
Keywords: blood flow, dissipative particle dynamics, red blood cell

1 INTRODUCTION

As a biological fluid, blood is comprised of deformable red blood cells, white blood cells, platelets and plasma. Red blood cells (RBCs), as the main composition of blood, determine the nature of blood rheology and their behaviors and largely affect the dynamics of the blood flow. The specific regime of the RBCs flow in blood vessels changes from large to small vessel sizes. In vivo experiments have observed that the RBCs advance in narrow capillaries in a single file surrounded with plasma under normal conditions, while the flow of RBCs in the larger microvessels is usually multifile and the transition to multifile flow is also attributed to an increase of hematocrit [1]. When flowing in a vessel, faster flow velocity promotes the migration of RBCs from the vessel wall toward the vessel center, resulting in a cell-rich central core and a cell-free layer formation near the wall and produces higher mean velocity of cells compared to plasma. This leads to a reduction of the tube hematocrit compared to the discharge hematocrit, which is called Fahraeus effect. In addition to the flow condition, many other factors including cell deformability, cell aggregability, hematocrit (the ratio of the RBC volume to the whole blood volume), vessel size and sedimentation strongly affects the rheological behavior of the blood flows in micro- and capillary vessel [2, 3]. The most impressive property of the relations is the reduction of the apparent blood viscosity with decreasing tube diameter, which was named Fahraeus–Lindqvist effect. This mainly results from the cell free layer with a lower viscosity compared to the cell-rich central core. Recent confocal microscopy with microfluidics has improved experimental measurements of RBCs behaviors in microvessels. However, owing to light scattering by RBCs and light absorption by hemoglobin, RBCs can be observed only under low hematocrit condition ($H_t < 20\%$) [4, 5].

Although the advances in computer and simulation technology facilitate investigations on blood flow, it is still challenging due to the computational expenses. A theoretical two-phase

ISSN: 2046-0546 (paper format), ISSN: 2046-0554 (online), http://www.witpress.com/journals
DOI: 10.2495/CMEM-V6-N2-303-313

model for the flow of blood in narrow tubes based on continuum approach developed by Sharan and Popel [6], where cell-free layer and cell-rich core have different viscosities, can capture the blood properties in vessels larger than 20 μm but lose its validity in tubes of 10~20 μm. Most existing numerical studies are limited to two-dimensional model. Sun and Munn [7] employed lattice Boltzmann approach to simulate the flow of rigid particle-like red blood cells. Zhang [8] further combined the lattice Boltzmann method with immersed boundary method to obtain the hemodynamic and hemorheological features through simulations of tens of two-dimensional deformable RBCs in channel flows. Nevertheless, two-dimensional modeling of the RBC suspensions cannot quantitatively capture the RBCs behaviors in blood flow.

In this study, dissipative particle dynamics method combined with a spring-based network cell model was employed to carry out simulations of blood flow in a tube. Then the simulation results of blood flow at different hematocrits in the tube ranging from 10 to 20μm will be given. Next, the cell distribution, flow velocity profile, Fahraeus effect, Fahraeus–Lindqvist effect and cell free layer thickness will be determined. Finally, summary and conclusions will be presented.

2 MODEL AND METHODS

2.1 Dissipative Particle Dynamics (DPD) method

DPD as a mesoscopic simulation technique has been used widely for computing the flow of complex fluids [9, 10]. Introductions to DPD method have been presented in detail [11–13]. In brief, each DPD particle i represents a soft lump of atoms and interacts with surrounding particles. The time evolution of DPD system is governed by Newton's equation of motion.

$$\begin{aligned} d\mathbf{r}_i &= \mathbf{v}_i dt \\ m_i d\mathbf{v}_i &= \sum_{j\neq i}\left(\mathbf{F}_{ij}^C - \gamma\omega(\mathrm{r}_{ij})(\mathbf{v}_{ij}\cdot\breve{\mathbf{r}}_{ij})\breve{\mathbf{r}}_{ij} + \sigma\omega(\mathrm{r}_{ij})^{1/2}\frac{\xi_{ij}}{\sqrt{dt}}\breve{\mathbf{r}}_{ij}\right)dt + \mathbf{F}_{ext}dt \end{aligned} \tag{1}$$

Here, m_i is the mass particle i, $\mathbf{r}_i$ and $\mathbf{v}_i$ are the position and velocity, $\mathbf{F}_{ij}^C$ is conservative force between dissipative particles i, j, $\breve{\mathbf{r}}_{ij} = \mathbf{r}_{ij}/r_{ij}$, $\mathbf{r}_{ij} = \mathbf{r}_i - \mathbf{r}_j$ and $\mathbf{v}_{ij} = \mathbf{v}_i - \mathbf{v}_j$. The coefficients γ and σ reflect the strength of dissipative and random forces, respectively. In addition, $\omega(r_{ij})$ is distance-dependent weight functions, and ξ_{ij} is a normally distributed random variable with zero mean, unit variance, and $\xi_{ij} = \xi_{ji}$. The random and dissipative forces form a thermostat and must satisfy the fluctuation-dissipation theorem in order for the DPD system to maintain the equilibrium temperature T [12], which leads to $\sigma^2 = 2\gamma k_B T$, k_B is Boltzmann constant. The first three terms are truncated beyond the cutoff radius r_c. $\mathbf{F}_{ext}$ is the external force acting upon the particle i, including the membrane force due to the cell deformation and the body force.

2.2 RBC membrane model

In simulations, the cell membrane is discretized into a collection of particles connected by elastic springs. A spring-based network model endowed with in-plane and bending energy as well as constraint of surface area and volume has been introduced by Boey [14] to describe RBC initially. A systematic coarse-grained procedure was introduced by Pivkin and

Karniadakis [15] to reduce the number of degrees of freedom dramatically in the RBC model. This coarse-grained model was further improved by Fedosov [16], yielding accurate mechanical response. The network nodes are connected by the springs with elastic energy as follows:

$$E_{in-plane} = \sum_{all\ edges} \left[\frac{k_B T l_{\max}}{4p} \frac{3x_l^{\,2} - 2x_l^{\,3}}{1 - x_l} + \frac{k_p}{(m-1)l^{m-1}} \right] \tag{2}$$

where $x_l = l / l_{\max} \in (0,1)$, $l_{\max}$ is the maximum spring extension, p is the persistence length. k_p is a POW force coefficient and m is a specified exponent [16].

The bending energy stored in the adjacent triangular elements is defined by

$$E_{bending} = \sum_{all\ triangle\ \ adjacents} k_{bend} \left[1 - \cos(\theta_{\alpha\beta} - \theta_0) \right] \tag{3}$$

where k_{bend} is a bending modulus; $\theta_{\alpha\beta}$ is the instantaneous angle formed between the outer normal vectors of two adjacent triangles α, β sharing the common edge; θ_0 is the spontaneous angle. To mimic area-incompressibility of the lipid bilayer and incompressibility of the internal fluid, the area and volume conservation constraints are included, which are given by

$$E_{area} + E_{volume} = \frac{k_{area}^{tot}(A^{tot} - A_0^{tot})^2}{2A_0^{tot}} + \sum_{all\ triangles} \frac{k_{area}(A - A_0)^2}{2A_0} + \frac{k_{volume}(V - V_0^{tot})^2}{2V_0^{tot}} \tag{4}$$

where k_{area}^{tot}, k_{area} and k_{volume} are constraint constants for global area, local area, and volume; A^{tot} and V are the instantaneous membrane area and the cell volume; A_0^{tot} and V_0^{tot} are their respective specified total area and volume values. A and A_0 are the instantaneous and initial local area.

Nodal forces are derived from the total energy as follows:

$$\mathbf{F}_i^{membrane} = -\partial E\{(\mathbf{r}_i)\}/\partial \mathbf{r}_i \tag{5}$$

3 RESULTS AND DISCUSSION

3.1 Modeling parameters

The blood flows in a tube ranging from 10 to 20 μm with a length of 50 μm were simulated. The blood was modeled as a suspension of RBCs. Each RBC consists of 640 particles and is 7.82 μm in diameter. It has a thickness at the thickest point of 2.5μm and a minimum thickness in the center of 1μm. The parameters of plasma and RBCs are listed in Table 1. The internal fluid of the cells has the same properties as the external plasma so that particle reflections at the membrane surface can be neglected. No-slip boundary condition was imposed near the wall and a periodic boundary condition was applied along the flow. To drive the flow, a uniform body force was applied to all particles in the flow direction, which is equivalent to the pressure gradient $\Delta P/L = \rho f$, where ΔP is the pressure drop over the tube length and ρ is the suspension's mass density. When the flow was turned on, the suspension began to flow and the RBCs deformed largely due to the shear flow. Widely known motions under shear flow for the RBCs involve tank-treading, tumbling and the transition between them. The

Table 1: Simulation parameters for cell membrane and plasma.

Parameter	Simulation	Physical values
Blood plasma density (ρ)	3	1.0×10^3 kg/m^3[17]
Blood plasma viscosity (μ)	20.4	1.2×10^{-3} Pa·s[17]
Temperature (T)	0.08486	310K
Membrane bending modulus (k_{bend})	4.565	2.3×10^{-19} J[16]
Time step (t)	0.002	0.00244 ms
Global area constraint constant (k_{area}^{tot})	5×10^4	3.35×10^{-3} N/m
Local area constraint constant (k_{area})	100	6.7 μN/m
Volume constraint constant (k_{volume})	5×10^4	3.35×10^{-3} N/m

behavior of the individual cell can be observed in the simulation of the blood flow in 20μm tube. As can be seen in Fig. 1, the cell located in the center is faster than the cells near the wall and the membrane marker shows the cell flows in the tank-treading motion. Each simulation was run for sufficient time to achieve steady state and data about velocity and cell distribution along the radius of the cross section were analyzed over the time at the steady state. The time to reach the steady state is around 0.5 s in physical units in this study. After this time, the properties of the blood flow were measured. The macro properties of the RBC suspensions flowing in different tubes concerning the discharge hematocrit, relative apparent viscosity and cell-free layer formed for different intercellular interaction strength will be discussed in the following sections.

3.2 RBC distribution and velocity profiles

In order to determine cell distribution in the cross section, the cylinder was divided into n narrow annuli S_i, for which $r_i < r < r_{i+1}$, r_0=0, r_n =R. R is the tube radius. The number density of the cell membrane particles belonging to each annulus was averaged over 0.1 s after the flow reached the steady state. The cell distribution was obtained through the cell membrane

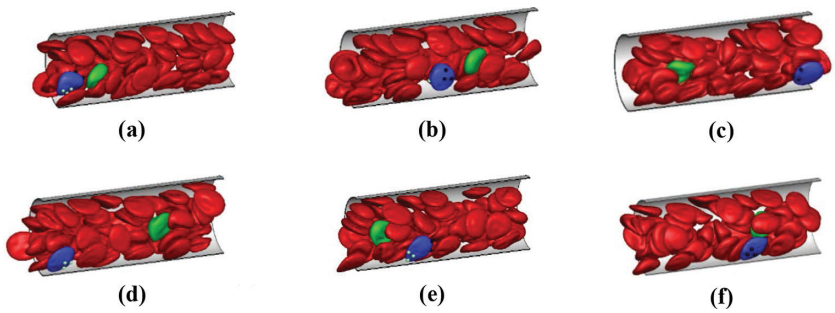

Figure 1: Snapshots of the flow developing process of RBCs in a tube with diameter of 20μm at t= 0.1342 s **(a)**, t= 0.1586 s **(b)**, t= 0.183 s **(c)**, t= 0.2074 s **(d)**, t= 0.2318 s **(e)**, and t= 0.2562 s **(f)**. The RBC suspension flows from left to right and the green RBC migrates toward the tube center and the blue cell flows near the wall. The cyan and black spheres are the membrane markers in the blue RBCs.

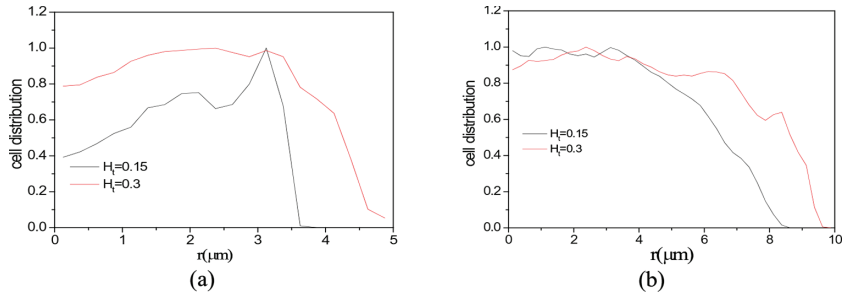

Figure 2: Radial distribution of RBCs in tubes of D = 10 μm (a) and D = 20 μm (b).

particles density in each annulus scaled by their maximum. This can be seen in Fig. 2, the distributions of RBCs in tubes of D = 10 μm and D = 20 μm for different hematocrits H_t are compared. Generally, cell concentration gradually increases toward the center of the tube. The similar cell distributions have been obtained in previous studies [18, 19]. It also showed that the distribution of cells for lower H_t values mainly concentrates on the center of tube and a larger cell free layer forms near the wall.

The velocity profile along the radius of the cross section is shown in Fig. 3. While the velocity profiles are parabolic in simulations with only plasma particles, illustrated in dashed lines in Fig. 3, in simulations with RBCs the velocity profiles are flat in the middle of the tube due to the high cell concentration. The influence of cell presence became stronger with increasing H_t value.

Table 2 lists the parameters about blood flow for different tube diameters, H_t values. Among them, the mean flow velocity is defined by

$$\overline{v} = Q / A = \int_A v(r) dA_c / A_c \tag{6}$$

where Q is volume flow rate and A_c is the area of cross section. The pseudo shear rate is represented by $\dot{\gamma} = \overline{v} / D$, and pressure gradient is expressed by $\Delta P / L$. v_p is the centerline velocity of plasma flow without RBCs. Most of the pseudo shear rates are above or around 30 s^{-1}, owing to the fact that the typical shear rates in *in vitro* and *in vivo* experiments are above 30 s^{-1}. And there is no significant effect of the aggregation on the cell free layer thickness for high shear rates, which were estimated at $\dot{\gamma} > 50 s^{-1}$ [2].

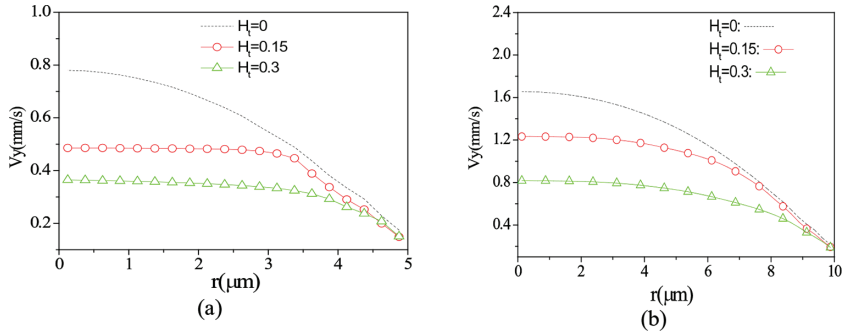

Figure 3: Velocity profile of RBCs flow in tubes of D = 10 μm (a) and D = 20 μm (b).

Table 2: Blood flow parameters for different hematocrit values and different tube Diameters. D is the tube diameter, H_t is the tube hematocrit, $\overline{\dot{\gamma}}$ is the pseudo shear rate, $\Delta P/L$ is the pressure gradient, v_p is the centerline velocity for the plasma flow without cells

D(μm)	H_t	$\overline{v}$ (mm/s)	$\overline{\dot{\gamma}}$ (1/s)	ΔP / L (Pa/m)	v_p (mm/s)
10	0.15	0.37	36.57	1.50E+05	0.78
10	0.3	0.29	29.02	1.50E+05	0.78
15	0.15	0.52	34.91	9.17E+04	1.08
15	0.3	0.38	25.55	9.17E+04	1.08
20	0.15	0.80	39.93	7.95E+04	1.66
20	0.3	0.56	28.16	7.95E+04	1.66

3.3 Fahraeus Effect and Fahraeus–Lindqvist Effect

The tendency of RBCs to migrate toward the center of the tube results in higher mean velocity of RBCs compared with the plasma. This leads to an increased value of discharge hematocrit, H_d, when the cells leave the tube exit, which was firstly discovered by Fahraeus in *in vitro* experiments of blood flow in glass tubes. The discharge hematocrit can be evaluated from the average cell velocity, $\overline{v}_c$, and mean flow velocity over all free DPD particles, v_m, over a time period after the flow is relatively steady:

$$H_d = \frac{\overline{v}_c}{v_m} H_t \tag{7}$$

An empirical description of *in vitro* experimental data for H_d as a function of H_t and diameter D was presented by Pries, Neuhaus [3], which is expressed by

$$\frac{H_t}{H_d} = H_d + (1 - H_d)(1 + 1.7e^{-0.35D} - 0.6e^{-0.01D}) \tag{8}$$

The simulated results were compared with this description for different tube diameters and H_t values, as shown in Fig. 4. Generally, a tendency of discharge hematocrit is $H_d > H_t$. A larger discrepancy between the simulation and empirical values can be found at $H_t = 0.3$

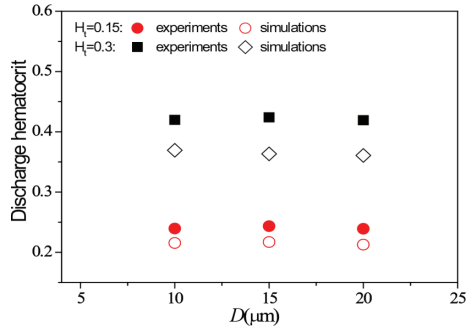

Figure 4: Comparison of discharge hematocrit between numerical results and empirical description in eqx. (8).

compared to the case at $H_t = 0.15$. This is mainly attributed to the fact that the flow rates employed are relatively lower than the experimental values.

Numerous *in vitro* experiments have been conducted to measure the apparent viscosity of blood in narrow glass. A decrease in the apparent blood viscosity with decreasing tube diameter was observed firstly by Fahraeus and Lindqvist in 1931. Pries, Neuhaus [3] provided the empirical relationship between the relative apparent viscosity η_{rel} and tube diameter D, discharge hematocrit H_d based on previous literature data regarding relative blood viscosity in tube flow *in vitro*.

$$\eta_{rel} = 1 + (\eta_{rel,0.45} - 1) \cdot \frac{(1 - H_d)^c - 1}{(1 - 0.45)^c - 1} \tag{9}$$

where $\eta_{rel,0.45}$ is the relative viscosity for a hematocrit of 0.45 and the parameter C is a function of diameter. They are given by empirical equations:

$$\eta_{rel,0.45} = 220 \cdot e^{-1.3D} + 3.2 - 2.44 \cdot e^{-0.06 D^{0.645}} \tag{10}$$

$$C = (0.8 + e^{-0.075 D}) \cdot \left(-1 + \frac{1}{1 + 10^{-11} \cdot D^{12}} \right) + \frac{1}{1 + 10^{-11} \cdot D^{12}} \tag{11}$$

For a steady flow of a homogeneous Newtonian fluid through a circular cylindrical tube, the volume flow rate Q is expressed by $Q = \pi \Delta P D^4 / 128 \eta L = \pi D^4 \overline{v} / 4$, where L is the tube length and η is the fluid viscosity. It is necessary to define an apparent viscosity of blood η_{app}, even if particulate nature of blood becomes significant in narrow tubes. Therefore, if ΔP, D, $\overline{v}$, L are measured or known, then the apparent viscosity can be calculated

$$\eta_{app} = \frac{\pi \Delta P D^4}{128 Q L} = \frac{\Delta P D^2}{32 \overline{v} L} \tag{12}$$

The value of η_{app} represents the viscosity of a homogeneous Newtonian fluid under the same flow rate in the tube with same tube length, diameter and pressure drop as the blood flow. So the relative apparent viscosity is defined as

$$\eta_{rel} = \frac{\eta_{app}}{\eta_s} \tag{13}$$

where η_s refers to the viscosity of the plasma.

Figure 5 presents the relative apparent viscosities obtained from the simulation results and compares these simulated values with the empirical fit to experiments [3]. The findings showed that the relative apparent viscosity decreases with the decrease in the tube diameter. It can be seen that the simulation results overpredict the relative apparent viscosity for $H_t = 0.3$, which is consistent with the results predicted in the discharge hematocrit in Fig. 4.

3.4 Cell Free Layer

As mentioned in the above sections, the tendency for cells to migrate toward the center of the tube leads to a thin layer of blood plasma without cells formed near the wall, which is so-called cell free layer [20] or cell-depleted wall layer [21]. The cell free layer plays a key

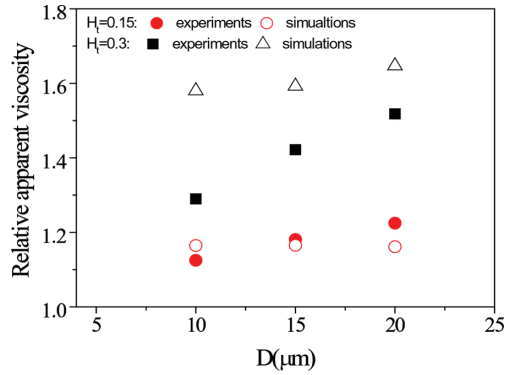

Figure 5: Comparison of relative apparent viscosity between simulation results and empirical description in eqx. (9).

role in lubrication and it is directly related to the Fahraeus–Lindqvist effect. In large tubes, the effect of the cell free layer is negligible, as its thickness is much smaller compared with the tube diameter. However, for the small tubes, the presence of the cell free layer significantly decreases the apparent viscosity. Due to the dispersive effect of RBCs in the blood flow, the thickness of the cell-free layer displayed spatial and temporal fluctuations in this study, which is similar to the findings in experimental investigations [22–24]. To determine the thickness of cell free layer, the distance between the outer edge of the cell and the wall was measured. Samples of CFL thickness were taken every 0.5 μm along the flow direction and per 9° in a counterclockwise direction from a single snapshot. And the thickness over all segments and a period time was averaged.

Figure 6 shows that cell free layer thickness for different tube diameters and H_t values. It is found that the thickness of cell free layer increases with the tube diameter and decreased H_t values. This trend is in a good agreement with previous experimental findings [24, 25]. The simulated cell free layer thickness values for high H_t value show a close agreement with the experiments. The discrepancy between simulated and experimental results are mainly due to the existence of glycocalyx layer of ~1 μm thickness [26] in *in vivo* experiments and

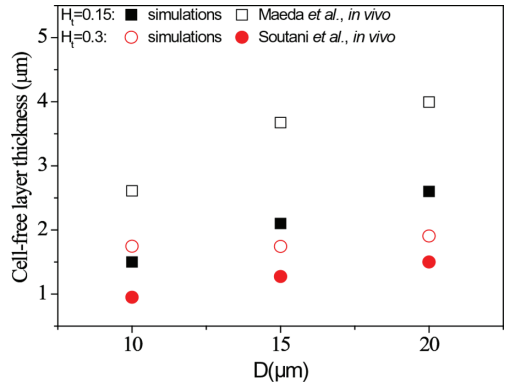

Figure 6: Cell free layer thickness for blood flows in tubes with different diameters and different hematocrits.

the difference in the flow rates. In *in vivo* experiments carried out by Maeda *et al.*, the aggregation was induced by adding Dextran T-70 to the RBCs suspension. An insignificant increase in the cell free layer thickness has been observed at a low concentration of Dextran T-70 [24].

4 CONCLUSIONS

The blood flow in microvessels for different tube diameters, H_t values were simulated using dissipative particle dynamics. During the process of blood flow development, RBCs near the tube wall migrate toward the center, creating a dense cell core and a thin cell free layer near the wall. In addition, the tank-treading motion of RBCs can be observed in our simulation results. Then the velocity profile of the blood flow and Fahraeus effect and Fahraeus–Lindqvist effect characterized by an increase of the discharge hematocrit Hd compared to tube hematocrit H_t and a decrease in the blood apparent viscosity with decreasing tube diameter were analyzed. The finding showed that the bluntness of velocity increased with increasing H_t. The simulated Hd values and relative apparent viscosity were compared with empirical fitting curves obtained from experiments. It was found that the simulated results are nearly in agreement with the experimental results. In conclusion, this flow model is able to capture the properties of blood flow and can be used to investigate the transport of other circulating cells or drug-carrying particles in the blood flow in the future.

ACKNOWLEDGEMENTS

Supports given by HKRGC PolyU 5202/13E, PolyU G-YBG9, NSFC 51276130, and NIH SC1 CA153325-01 are gratefully acknowledged.

REFERENCES

[1] Pries, A.R. & Secomb, T.W., Microvascular blood viscosity in vivo and the endothelial surface layer. *American Journal of Physiology-Heart and Circulatory Physiology*, **289**(6), pp. H2657–H2664, 2005. https://doi.org/10.1152/ajpheart.00297.2005

[2] Reinke, W., Gaehtgens, P. & Johnson, P.C., Blood-viscosity in small tubes - effect of shear rate, aggregation, and sedimentation. *American Journal of Physiology*, **253**(3), pp. H540–H547, 1987.

[3] Pries, A.R., Neuhaus, D. & Gaehtgens, P., Blood-viscosity in tube flow - dependence on diameter and hematocrit. *American Journal of Physiology*, **263**(6), pp. H1770–H1778, 1992.

[4] Lima, R., Ishikawa, T., Imai, Y., Takeda, M., Wada, S. & Yamaguchi, T., Measurement of individual red blood cell motions under high hematocrit conditions using a confocal micro-PTV system. *Annals of Biomedical Engineering*, **37**(8), pp. 1546–1559, 2009. https://doi.org/10.1007/s10439-009-9732-z

[5] Saadatmand, M., Ishikawa, T., Matsuki, N., Abdekhodaie, M.J., Imai, Y., Ueno, H. & Yamaguchi, T., Fluid particle diffusion through high-hematocrit blood flow within a capillary tube. *Journal of Biomechanics*, **44**(1), pp. 170–175, 2011. https://doi.org/10.1016/j.jbiomech.2010.09.004

[6] Sharan, M. & Popel, A.S., A two-phase model for flow of blood in narrow tubes with increased effective viscosity near the wall. *Biorheology*, **38**(5–6), pp. 415–428, 2001.

[7] Sun, C.H. & Munn, L.L., Particulate nature of blood determines macroscopic rheology: A 2-D lattice Boltzmann analysis. *Biophysical Journal*, **88**(3), pp. 1635–1645, 2005. https://doi.org/10.1529/biophysj.104.051151

[8] Zhang, J.F., Johnson, P.C. & Popel, A.S., An immersed boundary lattice Boltzmann approach to simulate deformable liquid capsules and its application to microscopic blood flows. *Physical Biology*, **4**(4), pp. 285–295, 2007.
https://doi.org/10.1088/1478-3975/4/4/005

[9] Warren, P.B., Vapor-liquid coexistence in many-body dissipative particle dynamics. *Physical Review E*, **68**(6), 2003.
https://doi.org/10.1103/physreve.68.066702

[10] Fan, X.J., Phan-Thien, N., Chen, S., Wu, X.H. & Ng, T.Y., Simulating flow of DNA suspension using dissipative particle dynamics. *Physics of Fluids*, **18**(6), 2006.
https://doi.org/10.1063/1.2206595

[11] Hoogerbrugge, P.J. & Koelman, J.M.V.A., Simulating microscopic hydrodynamic phenomena with dissipative particle dynamics. *Europhysics Letters*, **19**(3), pp. 155–160, 1992.
https://doi.org/10.1209/0295-5075/19/3/001

[12] Espanol, P., Hydrodynamics from dissipative particle dynamics. *Physical Review E*, **52**(2), pp. 1734–1742, 1995.
https://doi.org/10.1103/physreve.52.1734

[13] Groot, R.D. & Warren, P.B., Dissipative particle dynamics: Bridging the gap between atomistic and mesoscopic simulation. *Journal of Chemical Physics*, **107**(11), pp. 4423–4435, 1997.
https://doi.org/10.1063/1.474784

[14] Boey, S.K., Boal, D.H. & Discher, D.E., Simulations of the erythrocyte cytoskeleton at large deformation. I. Microscopic models. *Biophysical Journal*, **75**(3), pp. 1573–1583, 1998.
https://doi.org/10.1016/s0006-3495(98)74075-5

[15] Pivkin, I.V. & Karniadakis, G.E., Accurate coarse-grained modeling of red blood cells. *Physical Review Letters*, **101**(11), 2008.
https://doi.org/10.1103/physrevlett.101.118105

[16] Fedosov, D.A., Caswell, B. & Karniadakis, G.E., Systematic coarse-graining of spectrin-level red blood cell models. *Computer Methods in Applied Mechanics and Engineering*, **199**(29–32), pp. 1937–1948, 2010.
https://doi.org/10.1016/j.cma.2010.02.001

[17] Skalak, R., Chien, S. & Mates, R.E., *Handbook of bioengineering*. McGraw-Hill, New York, 1987.

[18] Jafari, A., Mousavi, S.M. & Kolari, P., Numerical investigation of blood flow. Part 1: In microvessel bifurcations. *Communications in Nonlinear Science and Numerical Simulation*, **13**(8), pp. 1615–1626, 2008.
https://doi.org/10.1016/j.cnsns.2006.09.017

[19] Alizadehrad, D., Imai, Y., Nakaaki, K., Ishikawa, T. & Yamaguchi, T., Parallel simulation of cellular flow in microvessels using a particle method. *Journal of Biomechanical Science and Engineering*, **7**(1), pp. 57–71, 2012.
https://doi.org/10.1299/jbse.7.57

[20] Kim, S., Ong, P.K., Yalcin, O., Intaglietta, M. & Johnson, P.C., The cell-free layer in microvascular blood flow. *Biorheology*, **46**(3), pp. 181–189, 2009.

[21] Sugihara-Seki, M. & Fu, B.M.M., Blood flow and permeability in microvessels. *Fluid Dynamics Research*, **37**(1–2), pp. 82–132, 2005.
https://doi.org/10.1016/j.fluiddyn.2004.03.006

[22] Kim, S., Kong, R.L., Popel, A.S., Intaglietta, M. & Johnson, P.C., Temporal and spatial variations of cell-free layer width in arterioles. *American Journal of Physiology-Heart and Circulatory Physiology*, **293**(3), pp. H1526–H1535, 2007. https://doi.org/10.1152/ajpheart.01090.2006

[23] Kim, S., Kong, R.L., Popel, A.S., Intaglietta, M. & Johnson, P.C., A computer-based method for determination of the cell-free layer width in microcirculation. *Microcirculation*, **13**(3), pp. 199–207, 2006. https://doi.org/10.1080/10739680600556878

[24] Maeda, N., Suzuki, Y., Tanaka, S. & Tateishi, N., Erythrocyte flow and elasticity of microvessels evaluated by marginal cell-free layer and flow resistance. *American Journal of Physiology-Heart and Circulatory Physiology*, **271**(6), pp. H2454–H2461, 1996.

[25] Soutani, M., Suzuki, Y., Tateishi, N. & Maeda, N., Quantitative-evaluation of flow dynamics of erythrocytes in microvessels - influence of erythrocyte aggregation. *American Journal of Physiology-Heart and Circulatory Physiology*, **268**(5), pp. H1959–H1965, 1995.

[26] Damiano, E.R., The effect of the endothelial-cell glycocalyx on the motion of red blood cells through capillaries. *Microvascular Research*, **55**(1), pp. 77–91, 1998. https://doi.org/10.1006/mvre.1997.2052